

# Geometric effects in the infinite-layer nickelates

F. Bernardini,<sup>1</sup> A. Bosin,<sup>1</sup> and A. Cano<sup>2</sup>

<sup>1</sup>*Dipartimento di Fisica, Università di Cagliari, IT-09042 Monserrato, Italy*

<sup>2</sup>*Univ. Grenoble Alpes, CNRS, Grenoble INP, Institut Néel, 25 Rue des Martyrs, 38042, Grenoble, France*

(Dated: October 27, 2021)

Geometric effects in the infinite-layer nickelates  $R\text{NiO}_2$  associated with the relative size of the  $R$ -site atom are investigated via first-principles calculations. We consider, in particular, the prospective  $\text{YNiO}_2$  material to illustrate the impact of these effects. We find that the presence of topotactic hydrogens can be precluded at the expense of an increase in both self-doping effect and  $e_g$  hybridization that deteriorates the cuprate-like electronic picture. Furthermore, we find that these geometric effects introduce a quantum critical point in the  $R\text{NiO}_2$  series. This implies a  $P4/mmm \leftrightarrow I4/mcm$  structural transformation associated to a  $A_3^+$  normal mode, according to which the oxygen squares undergo an in-plane rotation around Ni that alternates along  $c$ . We find that such a  $A_3^+$ -mode instability has a generic character in the infinite-layer nickelates and can be tuned via either the effective  $R$ -site atom size or epitaxial strain.

## I. INTRODUCTION

The infinite-layer nickelates  $R\text{NiO}_2$  ( $R$  = rare-earth element) have long been discussed as candidate materials for cuprate-like high- $T_c$  superconductivity [1–4]. Thus, the recent discovery of unconventional superconductivity in these systems has generated a substantial research attention [5–7]. Initially, superconductivity was observed in Sr-doped thin films for  $R = \text{Nd}$  but not for  $R = \text{La}$  [8]. This circumstance has raised the question of the role of the  $4f$  electrons [9] as well as of extrinsic factors such as the unintentional presence of topotactic hydrogen or apical oxygens, which have been argued to correlate with the structure [10, 11]. Examining the  $R\text{NiO}_2$  series for  $R$  from La to Lu as well as additional candidate materials for nickelate superconductivity has thus emerged as a consequential outlook [12–24]. At the same time, in analogy with their perovskite counterparts [25–27], the appearance of structural instabilities associated to the relative size of the  $R$  atom may also come into play as an additional key ingredient. To the best of our knowledge, this latter possibility remains unexplored so far.

In this context,  $\text{YNiO}_2$  provides a prospective model-case system combining the absence of  $4f$  electrons and geometric effects associated with a comparatively small  $R$  atom. Here, we introduce this system as a proxy to analyze the impact of these effects on the fundamental properties of the infinite-layer nickelates. Specifically, by means of first-principle calculations, we quantify the corresponding changes in both crystal structure and electronic properties, addressing also the likeliness of topotactic hydrogen insertion. Our analysis of geometrical effects further reveals the presence of a structural quantum critical point across the infinite-layer rare-earth nickelate series. We show that this structural instability is related to a distinct  $A_3^+$  soft-mode behavior that can be tuned via either the effective size of the atom at the  $R$  site or epitaxial strain.

## II. COMPUTATIONAL METHODS

The equilibrium structure and phonon calculations were performed using the QUANTUM ESPRESSO code [28]. Unless stated otherwise, we used the PBEsol pseudo-potentials from the SSSP library with a 75 (600) Ry cutoff for wavefunctions (density) [29, 30]. In addition, we also used norm-conserving PBEsol and PBE pseudopotentials from the Dojo library with a 115 (460) Ry cutoff for wavefunction (density) [31, 32]. The lattice parameters obtained for  $\text{LaNiO}_2$  and  $\text{YNiO}_2$  with these two sets of PBEsol pseudopotentials are essentially identical. However, significant differences are obtained with PBEsol vs PBE as discussed in the main text. In the case of the Pr - Eu elements, we restrict ourselves to PBE pseudopotentials in which the  $4f$  electrons of the are treated as core electrons. The phonon dispersion was computed using DFPT [33]. The Brillouin zone integration was performed using a  $16 \times 16 \times 20$   $k$ -mesh and a  $8 \times 8 \times 10$   $q$ -mesh was used to compute the dynamical matrix. Further, the optimized structural parameters were employed to compute the electronic structure properties using the all-electron code WIEN2K [34] based on the full-potential augmented plane-wave plus local orbitals method (APW+LO). We used muffin-tin radii of 2.5, 2.10, and 1.48 a.u. for the Y, Ni, and O atoms, respectively, and a plane-wave cutoff  $R_{\text{MT}}K_{\text{max}} = 7.0$ . The integration over the Brillouin zone was done using a Monkhorst-Pack mesh of  $11 \times 11 \times 14$   $k$ -points for the self-consistent calculations.

In addition, we performed magnetic calculations using both PBE and the local density approximation (LDA) [35] as the former is known to overestimate the tendency towards magnetic order, especially in metals. The magnetic solutions were obtained using different cells according to the magnetic order under consideration. For the ferromagnetic (FM) order we used the primitive tetragonal cell, while for the  $A$ -type antiferromagnetic (AFM) order with the spins of adjacent  $\text{NiO}_2$  planes pointing in opposite directions —*i.e.* FM planes stacked

AFM along  $c$ — we used a tetragonal cell encompassing 2 formula units. For the  $C$ -type AFM order —*i.e.* checkerboard order in-plane — we used a  $\sqrt{2} \times \sqrt{2} \times 1$  tetragonal cell encompassing 2 formula units, with  $a$  and  $b$ -axis rotated by  $45^\circ$  with respect to the primitive cell. For the  $G$ -type AFM with nearest-neighboring spins pointing in opposite directions (“full” AFM ordering) we used a  $\sqrt{2} \times \sqrt{2} \times 2$  body-centered tetragonal cell. Finally, we also considered the  $E$ -type AFM order where spins are aligned forming a double stripe structure using a base-centered orthorhombic cell encompassing 4 formula units.

### III. RESULTS

#### A. Structure

We first consider the ideal  $P4/mmm$  structure of the prospective nickelate  $\text{YNiO}_2$ . The optimized lattice parameters are  $a = 3.798 \text{ \AA}$  and  $c = 3.092 \text{ \AA}$ . Compared to  $\text{LaNiO}_2$ , the volume of the unit cell is reduced due to the smaller size of the Y cation. In fact, the  $a$  parameter is smaller compared to the values reported across the  $R\text{NiO}_2$  series ( $R = \text{La} - \text{Lu}$ ) while the parameter  $c$  is similar to the calculated for  $\text{ErNiO}_2$  [18, 19]. We note that this difference, however, is resolved when the PBE functional is used instead of PBEsol. In that case, we obtain  $a = 3.870 \text{ \AA}$  and  $c = 3.177 \text{ \AA}$ , which places  $\text{YNiO}_2$  right between  $\text{TbNiO}_2$  and  $\text{ErNiO}_2$  in terms of both  $a$  and  $c$  lattice parameters.

#### B. Topotactic hydrogen

Infinite-layer nickelates are typically obtained from their perovskite counterparts by means of topochemistry, using reducing agents such as  $\text{CaH}_2$ . This process, however, may lead to oxide-hydrides  $R\text{NiO}_2\text{H}$  instead, as concluded for  $R = \text{La}$  but not for Nd after partial substitution with Sr [10]. This suggests a link between the presence of topotactic hydrogen and the size of the rare-earth element that can be further verified by analyzing  $\text{YNiO}_2$ .

Thus, to determine whether the nickelates with smaller  $R$  atoms may host topotactic hydrogens, we first consider  $\text{YNiO}_2\text{H}$  with three possible configurations. Namely, with the H atom occupying either apical, interstitial or equatorial positions. The computed structures and relative energies are given in Table I. We find that the configuration in which the H sits at the apical positions is energetically favoured. We note that the same situation takes place in  $\text{LaNiO}_2$  [10]. The H binding energy  $E_B$  can then be computed from the corresponding total energies as [10]

$$E_B = E[\text{YNiO}_2] + E[\text{H}_2]/2 - E[\text{YNiO}_2\text{H}]. \quad (1)$$

Thus, we find that, contrary to  $\text{LaNiO}_2$ , the incorporation of H into  $\text{YNiO}_2$  is energetically unfavorable by

H position	$a$ (Å)	$b$ (Å)	$c$ (Å)	$\Delta E$ (eV/f.u.)
Apical	3.850	3.850	3.180	0
Interstitial	4.076	3.734	3.236	+2.38
Equatorial	3.830	3.830	3.486	+3.25

TABLE I. Lattice parameters and relative energy of  $\text{YNiO}_2\text{H}$  calculated for different positions of the H atom.

0.2 eV. This is in fact in tune with the trend previously obtained as a function of Sr-doping and strain [10]. Our results thus confirm that the  $R\text{NiO}_2$  nickelates are borderline systems where the H binding energy can change from positive to negative. In the case of  $(\text{La} \rightarrow \text{Y})\text{NiO}_2$ , topotactic hydrogen is avoided by means of a  $\text{Y}^{3+}$  cation that preserves the nominal 1+ oxidation state of the Ni atom.

#### C. Electronic properties

Fig. 1 shows the band structure and orbital-resolved density of states (DOS) of  $\text{YNiO}_2$  in the  $P4/mmm$  structure. The main features near the Fermi level are associated to the Ni- $3d$  bands. These features can be traced back to the nominal  $3d^9$  configuration of the  $\text{Ni}^{1+}$  as in  $\text{LaNiO}_2$ . The splitting between the  $e_g = \{d_{x^2-y^2}, d_{z^2}\}$  states, however, is considerably reduced. At the same time, there is a sizable self-doping from the ideal  $d^9$  configuration which, despite the reduced polarizability of the Y ion, is visibly enhanced compared to  $\text{LaNiO}_2$ . Such a self-doping originates from a Y- $4d$  derived band, which has an increased hybridization not only with Ni- $3d_{z^2}$  but also with O- $2p$  states. In fact the width of the O- $2p$  bands increases which makes the contribution of the O- $2p$  states to the DOS near the Fermi level slightly higher compared to  $\text{LaNiO}_2$ . These modifications result from the reduced lattice parameters of  $\text{YNiO}_2$ , and are compatible with the reported in [18] for  $\text{LaNiO}_2$  as a function of the in-plane lattice constant. Also, the presence of the two larger electron pockets at  $\Gamma$  and A is in tune with the reported in [19].

These changes in the electronic structure modify the tendency towards magnetism as summarized in Table II. Specifically, our calculations with FM and A-AFM initial configurations converged but yielded a vanishing magnetic moment. The rest of configurations resulted in metastable states at the LDA level. We note that, however, the magnetization energies are relatively small and the situation in fact changes when the PBE functional is used since the tendency towards magnetism is generally overestimated in this case. Specifically, the energy of these configurations becomes lower than the non-magnetic solution by  $-13.76 \text{ meV/Ni}$ ,  $-15.04 \text{ meV/Ni}$  and  $-22.18 \text{ meV/Ni}$  for the  $E$ -,  $C$ - and  $G$ -AFM configurations respectively. The Ni magnetic moment is  $0.5 \mu_B$  in all the three cases.

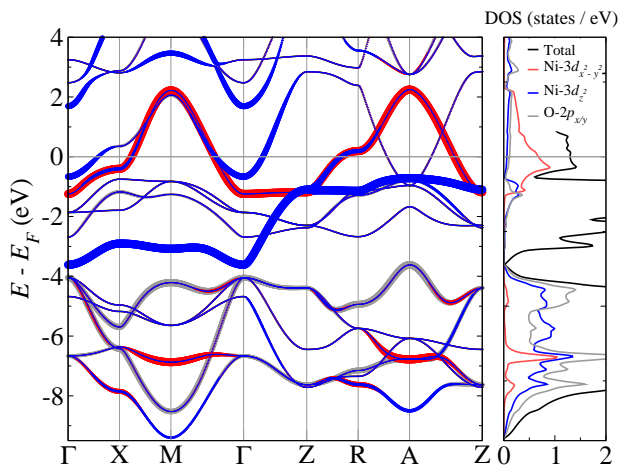


FIG. 1. Band structure along the high-symmetry directions of the Brillouin zone and density of states of  $\text{YNiO}_2$  in the  $P4/mmm$  structure.

	$\Delta E$ (meV/Ni)	$\mu_{\text{Ni}}$ ( $\mu_B$ )
$G$ -AFM	+2.98	0.30
$E$ -AFM	+1.18	0.14
$C$ -AFM	+0.27	0.06
$A$ -AFM	-	-
FM	-	-

TABLE II. Energy difference with respect to the non-magnetic solution and magnetic moment of the Ni atom for different magnetic configurations of  $\text{YNiO}_2$  obtained in LDA calculations.

#### D. $P4/mmm \rightarrow I4/mcm$ structural distortion & epitaxial strain

Next, we address the stability of the  $P4/mmm$  structure of the infinite-layer  $R\text{NiO}_2$  nickelates when the size of the  $R$  atom is reduced. The Goldschmidt tolerance factor is a well known geometric indicator of the stability of cubic perovskites. In the tetragonal infinite-layer case, there is an analogous ‘no rattle limit’ that can be inferred from the ratio of ionic radii also. Accordingly, for  $R = \text{Y}$ , we note that the ionic-radius ratio  $r_{\text{Y}}/r_{\text{O}}$  in 8-fold coordination is 0.718, and hence below such a limit (0.732). In fact, the calculated Y-O distance in  $\text{YNiO}_2$  is slightly larger than the sum of the corresponding radii. Consequently, the system may be prone to structural instabilities according to Pauling’s rules.

To confirm this, we considered possible distortions of the  $P4/mmm$  structure. The phonon spectrum, in particular, reveals a dynamical instability at the A point of the Brillouin zone (see Fig. 2). In fact, we further find that the total energy is minimized in the  $I4/mcm$  structure illustrated in Fig. 3. The optimized lattice parameters are  $a = 5.390 \text{ \AA}$  and  $c = 6.376 \text{ \AA}$ , with the parameter  $x_{\text{O}} = 0.03873$  determining the oxygen positions at the  $8h$  Wyckoff sites. As discussed above, this

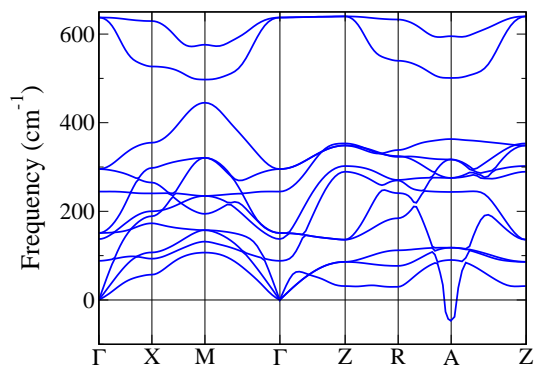


FIG. 2. Phonon spectrum of  $\text{YNiO}_2$  computed in the optimized  $P4/mmm$  structure. The spectrum reveals a weak instability at A [ $\mathbf{q} = (1/2, 1/2, 1/2)$ ] associated to a  $A_3^+$  normal mode.

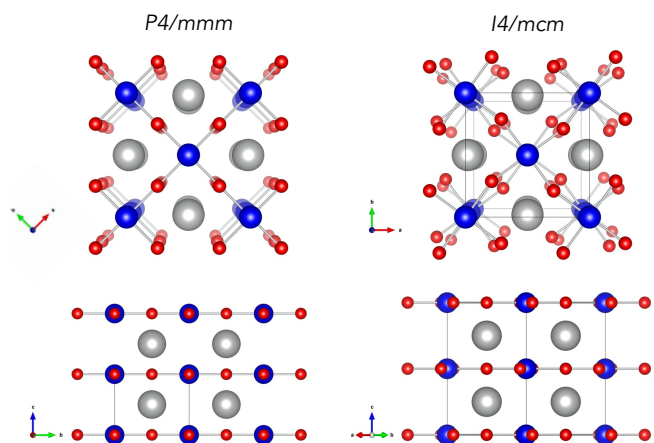


FIG. 3. Top and side views of the ideal  $P4/mmm$  and distorted  $I4/mcm$  structures of the infinite-layer nickelates  $R\text{NiO}_2$ . Gray, blue and red balls indicate  $R$ , Ni and O atoms respectively.

$P4/mmm \rightarrow I4/mcm$  instability can be ascribed to the presence of a  $R$  atom that is too small (i.e. a geometric effect). In fact, we find a gradual softening of the  $A_3^+$  phonon across the series that eventually reveals the dynamical instability of the  $P4/mmm$  structure as summarized in Table III. Specifically, while the  $R = \text{La}$ ,  $\text{Pr}$ , and  $\text{Nd}$  members remain stable, the structural instability emerges for smaller  $R$  elements. At the same time, we obtain different  $A_3^+$ -mode frequencies depending on the exchange-correlation —PBE vs PBEsol— functional that is employed. Thus, while the existence of a critical  $R$  size is clear from the calculated trend, we could not conclude its precise value.

In any case, the structural instability of the  $P4/mmm$  phase is relatively weak. In fact, for  $\text{YNiO}_2$ , the difference in energy between the  $P4/mmm$  and the  $I4/mcm$  structures is only 45 meV per formula unit. Thus, we considered the influence of epitaxial strain since this may prevent the in-plane oxygen rotations within the  $\text{NiO}_2$  layers. Epitaxial strain  $\epsilon$  is modeled by changing the in-

	$a$ (Å)	$c$ (Å)	$\omega_{A_3^+}$ (cm $^{-1}$ )
La	3.939 (3.880)	3.398 (3.352)	132.0 (178.0)
Pr	3.920	3.355	119.7
Nd	3.905	3.310	95.2
Sm	3.880	3.237	$i$ 38.1
Eu	3.870	3.207	$i$ 82.6
Y	3.850 (3.798)	3.144 (3.092)	$i$ 130.1 ( $i$ 52.5)

TABLE III. Optimized lattice parameters and frequency of the  $A_3^+$  mode for different  $R\text{NiO}_2$  systems in the  $P4/mmm$  structure obtained with the PBE exchange-correlation functional (the values between parenthesis correspond to the PBEsol functional). Imaginary frequencies indicate the dynamical instability of the  $P4/mmm$  structure.

plane lattice parameter and relaxing the structure in the  $c$  direction [ $\epsilon = (a - a_0)/a_0$ , where  $a_0$  is the initial (relaxed) lattice constant]. The top panel in Fig. 4 shows the calculated  $c$  parameter as a function of epitaxial strain in the  $P4/mmm$  structure. The  $c$  parameter increases by decreasing the lattice constant  $a$ , and in this sense counteracts the La  $\rightarrow$  Y substitution. This behavior is standard and can be expected across the  $R\text{NiO}_2$  series also. The overall modification of the structure, however, remains dominated by the relative changes imposed in  $a$ . Consequently, compressive strain can be expected to reduce the Y ‘rattle’ and thereby to stabilize the  $P4/mmm$  structure.

The bottom panel of Fig. 4 shows the computed frequency of the soft  $A_3^+$  mode as a function of epitaxial strain. As we see, this mode hardens for compressive strain so that the corresponding instability disappears for  $\epsilon \lesssim -0.7\%$ . This confirms that the in-plane compression obtained via epitaxial strain overcomes the out-of-plane expansion, thereby providing a direct handle to stabilize the  $P4/mmm$  structure. Conversely, we find that tensile strain enhances the  $A_3^+$ -mode instability. We have performed additional calculations for other  $R\text{NiO}_2$  systems. These calculations reveal that this soft-mode behavior as a function of epitaxial strain is in fact a generic feature of the infinite-layer rare-earth nickelates. Accordingly, the  $I4/mcm$  structure with the O-square rotations should be expected even in  $\text{LaNiO}_2$  under high enough tensile strain.

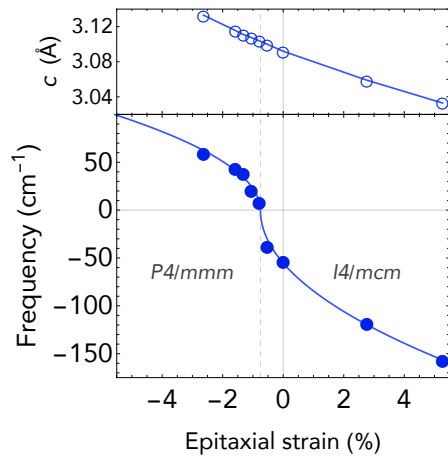


FIG. 4. Out-of-plane lattice parameter  $c$  (top panel) and frequency of the soft  $A_3^+$  mode (bottom panel) of  $\text{YNiO}_2$  calculated in the  $P4/mmm$  structure as a function of epitaxial strain. Negative values correspond to imaginary frequencies indicating the dynamical instability towards the  $I4/mcm$  structure. Compressive strain  $\lesssim -0.7\%$  tends to stabilize the  $P4/mmm$  structure without the rotation of the O squares.

#### IV. SUMMARY

In summary, we have investigated geometric effects in the infinite-layer rare-earth nickelates by means of first principles calculations. By considering the prospective material  $\text{YNiO}_2$ , we have confirmed that these effects can have a decisive influence on the actual reduction of their perovskite precursors since they can prevent the presence of topotactic hydrogen. However, the price to pay is the substantial modification of the electronic properties, which qualitatively deviate from the ideal cuprate-like case. Specifically, both the self-doping and the  $e_g$  hybridization —*i.e.*, the 3D character of the system— is enhanced while tendency towards magnetic order is weakened. Furthermore, we have shown that there exists a structural quantum critical point underneath the  $R\text{NiO}_2$  series. Specifically, we have found that the original  $P4/mmm$  structure eventually becomes unstable by either reducing the size of the  $R$  atom or under high-enough epitaxial tensile strain. This gives rise to a new  $I4/mcm$  superstructure with spontaneous, in-plane rotations of the oxygen squares according to a  $A_3^+$  soft-mode distortion. Interestingly, this structural instability is fundamentally different from its counterpart in the perovskite nickelates where the  $A_3^+$  mode is totally passive without contributing to their overall distortion [25–27]. In the infinite-layer nickelates, where the apical oxygens are absent, the  $A_3^+$ -mode becomes the main driver of their  $P4/mmm \leftrightarrow I4/mcm$  structural transformation instead. At the same time, we note that this instability is also different from the out-of-plane oxygen buckling reported for  $\text{CaCuO}_2$  [36]. Thus, our work establishes new links between geometric effects and fundamental properties of

the infinite-layer nickelates and we expect that our findings will motivate further investigations.

*Note added.* After the completion of this work, there appeared the preprint [37] reporting on the  $P4/mmm \rightarrow I4/mcm$  instability also.

## ACKNOWLEDGMENTS

F.B. acknowledges support from Cineca ISCRA-C project "IsC78-NICKSUP-HP10C91RDL".

- 
- [1] M. Hayward, M. Green, M. Rosseinsky, and J. Sloan, *Journal of the American Chemical Society* **121**, 8843 (1999).
- [2] V. I. Anisimov, D. Bukhvalov, and T. M. Rice, *Phys. Rev. B* **59**, 7901 (1999).
- [3] K.-W. Lee and W. E. Pickett, *Phys. Rev. B* **70**, 165109 (2004).
- [4] M. R. Norman, *Physics* **13**, 85 (2020).
- [5] A. S. Botana, F. Bernardini, and A. Cano, *JETP* **159**, 711 (2021), [arXiv:2012.02764](#).
- [6] J. Zhang and X. Tao, [arXiv:2103.06674](#).
- [7] Y. Nomura and R. Arita, [arXiv:2107.12923](#).
- [8] D. Li, K. Lee, B. Y. Wang, M. Osada, S. Crossley, H. R. Lee, Y. Cui, Y. Hikita, and H. Y. Hwang, *Nature (London)* **572**, 624 (2019).
- [9] M.-Y. Choi, K.-W. Lee, and W. E. Pickett, *Phys. Rev. B* **101**, 020503 (2020).
- [10] L. Si, W. Xiao, J. Kaufmann, J. M. Tomczak, Y. Lu, Z. Zhong, and K. Held, *Phys. Rev. Lett.* **124**, 166402 (2020).
- [11] F. Bernardini and A. Cano, *Journal of Physics: Materials* **3**, 03LT01 (2020).
- [12] M. Osada, B. Y. Wang, B. H. Goodge, S. P. Harvey, K. Lee, D. Li, L. F. Kourkoutis, and H. Y. Hwang, *Advanced Materials*, 2104083 (2021).
- [13] S. W. Zeng, C. J. Li, L. E. Chow, Y. Cao, Z. T. Zhang, C. S. Tang, X. M. Yin, Z. S. Lim, J. X. Hu, P. Yang, and A. Ariando, [arXiv:2105.13492](#).
- [14] M. Osada, B. Y. Wang, B. H. Goodge, K. Lee, H. Yoon, K. Sakuma, D. Li, M. Miura, L. F. Kourkoutis, and H. Y. Hwang, *Nano Letters* **20**, 5735–5740 (2020).
- [15] H. Lin, D. Jakub Gawryluk, Y. M. Klein, S. Huangfu, E. Pomjakushina, F. von Rohr, and A. Schilling, [arXiv:2104.14324](#).
- [16] C. He, X. Ming, Q. Li, X. Zhu, J. Si, and H.-H. Wen, [arXiv:2010.11777](#).
- [17] A. S. Botana, V. Pardo, and M. R. Norman, *Phys. Rev. Materials* **1**, 021801 (2017).
- [18] J. Kapeghian and A. S. Botana, *Phys. Rev. B* **102**, 205130 (2020).
- [19] E. Been, W.-S. Lee, H. Y. Hwang, Y. Cui, J. Zaanen, T. Devereaux, B. Moritz, and C. Jia, *Phys. Rev. X* **11**, 011050 (2021).
- [20] M. Hirayama, T. Tadano, Y. Nomura, and R. Arita, *Phys. Rev. B* **101**, 075107 (2020).
- [21] F. Bernardini, V. Olevano, X. Blase, and A. Cano, *J. Phys. Materials* **3**, 035003 (2020).
- [22] F. Bernardini, A. Demourgues, and A. Cano, *Phys. Rev. Materials* **5**, L061801 (2021).
- [23] Z. Li, W. Guo, T. T. Zhang, J. H. Song, T. Y. Gao, Z. B. Gu, and Y. F. Nie, *APL Materials* **8**, 091112 (2020).
- [24] G. A. Pan, D. Ferenc Segedin, H. LaBollita, Q. Song, E. M. Nica, B. H. Goodge, A. T. Pierce, S. Doyle, S. Novakov, D. Córdova Carrizales, A. T. N'Diaye, P. Shafer, H. Paik, J. T. Heron, J. A. Mason, A. Yacoby, L. F. Kourkoutis, O. Erten, C. M. Brooks, A. S. Botana, and J. A. Mundy, [arXiv:2109.09726](#).
- [25] A. Mercy, J. Bieder, J. Íñiguez, and P. Ghosez, *Nature Comm.* **8**, 1677 (2017).
- [26] J. Vargignon, M. N. Grisolia, J. Íñiguez, A. Barthélémy, and M. Bibes, *npj Quantum Materials* **2**, 21 (2017).
- [27] D. J. Gawryluk, Y. M. Klein, T. Shang, D. Sheptyakov, L. Keller, N. Casati, P. Lacorre, M. T. Fernández-Díaz, J. Rodríguez-Carvajal, and M. Medarde, *Phys. Rev. B* **100**, 205137 (2019).
- [28] P. Giannozzi and *et al.*, *J. Phys.: Condens. Matter* **21**, 395502 (2009).
- [29] J. P. Perdew, A. Ruzsinszky, G. I. Csonka, O. A. Vydrov, G. E. Scuseria, L. A. Constantin, X. Zhou, and K. Burke, *Phys. Rev. Lett.* **100**, 136406 (2008).
- [30] G. Prandini, A. Marrazzo, I. E. Castelli, N. Mounet, and N. Marzari, *npj Computational Materials* **4**, 72 (2018).
- [31] D. R. Hamann, *Phys. Rev. B* **88**, 085117 (2013).
- [32] M. van Setten, M. Giantomassi, E. Bousquet, M. Verstraete, D. Hamann, X. Gonze, and G.-M. Rignanese, *Comput. Phys. Commun.* **226**, 39 (2018).
- [33] S. Baroni, P. Giannozzi, and A. Testa, *Phys. Rev. Lett.* **58**, 1861 (1987).
- [34] P. Blaha, K. Schwarz, G. Madsen, D. Kvasnicka, J. Luitz, R. Laskowski, F. Tran, and L. D. Marks, WIEN2k, An Augmented Plane Wave + Local Orbitals Program for Calculating Crystal Properties (Karlheinz Schwarz, Techn. Universität Wien, Austria), 2018. ISBN 3-9501031-1-2.
- [35] J. P. Perdew and A. Zunger, *Phys. Rev. B* **23**, 5048 (1981).
- [36] O. K. Andersen, S. Y. Savrasov, O. Jepsen, and A. I. Liechtenstein, *J. Low Temp. Phys.* **105**, 285–304 (1996).
- [37] C. Xia, J. Wu, Y. Chen, and H. Chen, [arXiv:2110.12405](#).